

A DAMA/Libra-phase2 analysis in terms of WIMP-quark and WIMP-gluon effective interactions up to dimension seven

Sunghyun Kang, Stefano Scopel, Gaurav Tomar,

Department of Physics, Sogang University, Seoul, Korea, 121-742

E-mail: francis735@naver.com, scopel@sogang.ac.kr, tomar@sogang.ac.kr

Abstract. We analyze the DAMA/Libra-phase2 modulation result using a basis of 16 effective operators describing the WIMP interaction with photons, gluons and quarks up to mass dimension seven. For each operator we fix the effective theory at the scale of 2 GeV and parametrize WIMP-quark interactions in terms of two independent couplings for up-type and down-type quarks. We discuss the connection with the non-relativistic limit of the effective theory in terms of operators invariant by Galilean transformations, and the impact of the ensuing momentum-dependent Wilson coefficients due to long-range interactions or light meson poles. Most relativistic operators yield a good fit of the DAMA modulation effect, although for parameters excluded by the constraints from XENON1T and PICO60.

Contents

1	Introduction	1
2	WIMP rates in effective models	2
3	Analysis	8
4	Conclusions	17

1 Introduction

The Large Hadron Collider (LHC) did not find so far any evidence of physics beyond the Standard Model, excluding the most straightforward realizations of Supersymmetry or Large Extra Dimensions that provided the most popular Dark Matter (DM) candidates. As a consequence, model-independent approaches have become increasingly popular to interpret DM search experiments [1–20]. In particular, the DAMA modulation excess may serve as a benchmark to develop and test such approaches [21–24]. It has reached a more than 12σ statistical significance and for it no explanation alternative to a WIMP signal has been found so far, while experiments trying to replicate it using the same sodium iodide target material have only now started to reach the required sensitivity [25–27]. Nevertheless, in spite of its potential relevance, a completely model-independent assessment of such result against the null outcomes of other experiments is still not available after almost 20 years of its appearance.

In order to address this aspect the DAMA result has been analyzed parametrizing the WIMP–nucleus interaction in terms of the non-relativistic operators allowed by Galilean invariance [28, 29] including all interferences [24, 30], finding that, in the case of a Maxwellian WIMP velocity distribution, the tension between the WIMP interpretation of the modulation effect and the constraints from other null results persists. The same result was found assuming dominance of one non-relativistic operator at a time [23]. In all such analyses, however, no explicit momentum dependence of the Wilson coefficients of the Non Relativistic (NR) Effective Field Theory (EFT) was assumed. If, in alternative, the WIMP-nucleus interaction is parameterized in terms of a relativistic WIMP–quark, WIMP-photon or WIMP–gluon effective theory [20, 31–35] (i) only a few of the non-relativistic operators allowed by Galilean invariance actually appear in the non-relativistic limit ; (ii) usually, more than one operator appears in the non-relativistic limit, including interference terms; (iii) the couplings of the non-relativistic theory may acquire an explicit momentum dependence due to a long-range component of the relativistic coupling or because of light meson poles. In this case an assessment on the DAMA fit, including the latest DAMA/Libra phase2 low-threshold analysis, has not been provided yet. To fill this gap

in the present paper we wish to extend the analysis of Ref. [23] with an assessment of the DAMA/Libra–phase2 modulation result using a basis of 16 effective operators describing the WIMP effective interaction with photons, gluons and quarks up to mass dimension seven:

$$\mathcal{L}_\chi = \sum_q \sum_{a,d} \mathcal{C}_{a,q}^{(d)} \mathcal{Q}_{a,q}^{(d)} + \sum_{b,d} \mathcal{C}_b^{(d)} \mathcal{Q}_b^{(d)}, \quad (1.1)$$

In particular, we assume the same set of operators discussed in [20] and analyzed in [36]. Analyses on similar sets of relativistic DM effective operators can also be found in [31–34].

The paper is organized as follows: in Section 2 we list the $\mathcal{Q}_{a,q}^{(d)}$, $\mathcal{Q}_b^{(d)}$ effective operators and outline how we calculate the corresponding DM Direct Detection (DD) expected rates; Section 3 contains our quantitative results; we draw our conclusions in Section 4.

2 WIMP rates in effective models

We consider the two dimension-five operators:

$$\mathcal{Q}_1^{(5)} = \frac{e}{8\pi^2} (\bar{\chi} \sigma^{\mu\nu} \chi) F_{\mu\nu}, \quad \mathcal{Q}_2^{(5)} = \frac{e}{8\pi^2} (\bar{\chi} \sigma^{\mu\nu} i \gamma_5 \chi) F_{\mu\nu}, \quad (2.1)$$

where $F_{\mu\nu}$ is the electromagnetic field strength tensor and χ is the DM field, assumed here to be a Dirac particle. Such operators correspond, respectively, to magnetic–dipole and electric–dipole DM and imply a long–range interaction [37]¹. The dimension-six operators are

$$\begin{aligned} \mathcal{Q}_{1,q}^{(6)} &= (\bar{\chi} \gamma_\mu \chi) (\bar{q} \gamma^\mu q), \quad \mathcal{Q}_{2,q}^{(6)} = (\bar{\chi} \gamma_\mu \gamma_5 \chi) (\bar{q} \gamma^\mu q), \\ \mathcal{Q}_{3,q}^{(6)} &= (\bar{\chi} \gamma_\mu \chi) (\bar{q} \gamma^\mu \gamma_5 q), \quad \mathcal{Q}_{4,q}^{(6)} = (\bar{\chi} \gamma_\mu \gamma_5 \chi) (\bar{q} \gamma^\mu \gamma_5 q), \end{aligned} \quad (2.2)$$

and we also include the following dimension-seven operators: namely:

$$\begin{aligned} \mathcal{Q}_1^{(7)} &= \frac{\alpha_s}{12\pi} (\bar{\chi} \chi) G^{a\mu\nu} G_{\mu\nu}^a, \quad \mathcal{Q}_2^{(7)} = \frac{\alpha_s}{12\pi} (\bar{\chi} i \gamma_5 \chi) G^{a\mu\nu} G_{\mu\nu}^a, \\ \mathcal{Q}_3^{(7)} &= \frac{\alpha_s}{8\pi} (\bar{\chi} \chi) G^{a\mu\nu} \tilde{G}_{\mu\nu}^a, \quad \mathcal{Q}_4^{(7)} = \frac{\alpha_s}{8\pi} (\bar{\chi} i \gamma_5 \chi) G^{a\mu\nu} \tilde{G}_{\mu\nu}^a, \\ \mathcal{Q}_{5,q}^{(7)} &= m_q (\bar{\chi} \chi) (\bar{q} q), \quad \mathcal{Q}_{6,q}^{(7)} = m_q (\bar{\chi} i \gamma_5 \chi) (\bar{q} q), \\ \mathcal{Q}_{7,q}^{(7)} &= m_q (\bar{\chi} \chi) (\bar{q} i \gamma_5 q), \quad \mathcal{Q}_{8,q}^{(7)} = m_q (\bar{\chi} i \gamma_5 \chi) (\bar{q} i \gamma_5 q), \\ \mathcal{Q}_{9,q}^{(7)} &= m_q (\bar{\chi} \sigma^{\mu\nu} \chi) (\bar{q} \sigma_{\mu\nu} q), \quad \mathcal{Q}_{10,q}^{(7)} = m_q (\bar{\chi} i \sigma^{\mu\nu} \gamma_5 \chi) (\bar{q} \sigma_{\mu\nu} q). \end{aligned} \quad (2.3)$$

¹The anapole coupling $(\bar{\chi} \gamma^\mu \gamma_5 \chi) \partial^\nu F_{\mu\nu}$ leads instead to an effective contact interaction. The DAMA result was already analyzed in the cases of magnetic dipole and anapole DM in [38], while a recent analysis of anapole DM is also provided in [39].

$\mathcal{O}_1 = 1_\chi 1_N$	$\mathcal{O}_9 = i\vec{S}_\chi \cdot (\vec{S}_N \times \frac{\vec{q}}{m_N})$
$\mathcal{O}_2 = (v^\perp)^2$	$\mathcal{O}_{10} = i\vec{S}_N \cdot \frac{\vec{q}}{m_N}$
$\mathcal{O}_3 = i\vec{S}_N \cdot (\frac{\vec{q}}{m_N} \times \vec{v}^\perp)$	$\mathcal{O}_{11} = i\vec{S}_\chi \cdot \frac{\vec{q}}{m_N}$
$\mathcal{O}_4 = \vec{S}_\chi \cdot \vec{S}_N$	$\mathcal{O}_{12} = \vec{S}_\chi \cdot (\vec{S}_N \times \vec{v}^\perp)$
$\mathcal{O}_5 = i\vec{S}_\chi \cdot (\frac{\vec{q}}{m_N} \times \vec{v}^\perp)$	$\mathcal{O}_{13} = i(\vec{S}_\chi \cdot \vec{v}^\perp)(\vec{S}_N \cdot \frac{\vec{q}}{m_N})$
$\mathcal{O}_6 = (\vec{S}_\chi \cdot \frac{\vec{q}}{m_N})(\vec{S}_N \cdot \frac{\vec{q}}{m_N})$	$\mathcal{O}_{14} = i(\vec{S}_\chi \cdot \frac{\vec{q}}{m_N})(\vec{S}_N \cdot \vec{v}^\perp)$
$\mathcal{O}_7 = \vec{S}_N \cdot \vec{v}^\perp$	$\mathcal{O}_{15} = -(\vec{S}_\chi \cdot \frac{\vec{q}}{m_N})((\vec{S}_N \times \vec{v}^\perp) \cdot \frac{\vec{q}}{m_N})$
$\mathcal{O}_8 = \vec{S}_\chi \cdot \vec{v}^\perp$	

Table 1. Non-relativistic Galilean invariant operators for dark matter with spin 1/2.

In the equations above $q = u, d, s$ denote the light quarks, $G_{\mu\nu}^a$ is the QCD field strength tensor, while $\tilde{G}_{\mu\nu} = \frac{1}{2}\varepsilon_{\mu\nu\rho\sigma}G^{\rho\sigma}$ is its dual, and $a = 1, \dots, 8$ are the adjoint color indices. In the following we will also assume that all the operators listed in Eqs.(2.1)–(2.3) conserve flavor.

In the following Section we will show our results parametrizing each coupling $\mathcal{C}^{(d)} = \mathcal{C}_{a,q}^{(d)}, \mathcal{C}_b^{(d)}$ in Eq. (1.1) with the effective scale $\tilde{\Lambda}$:

$$\mathcal{C}^{(d)} \equiv \frac{1}{\tilde{\Lambda}^{d-4}}. \quad (2.4)$$

In particular, for the interactions with quarks we factorize the coupling $\mathcal{C}_{up}^{(d)} = 1/\tilde{\Lambda}^{d-4}$ with the up quark and assume a common value $\mathcal{C}_{down}^{(d)} = \mathcal{C}_{strange}^{(d)}$ for two remaining couplings with the down and strange quarks, introducing the additional parameter:

$$r = \mathcal{C}_{down}^{(d)}/\mathcal{C}_{up}^{(d)}. \quad (2.5)$$

The non-relativistic limit of each of the operators of Eqs. (2.1–2.3) yields a linear combination of the operators that parameterize the most general effective Hamiltonian for the WIMP–nucleus interaction that complies with Galilean symmetry, containing at most 15 terms in the case of a spin-1/2 particle [28, 29]:

$$\mathcal{H}(\mathbf{r}) = \sum_{\tau=0,1} \sum_{j=1}^{15} c_j^\tau \mathcal{O}_j(\mathbf{r}) t^\tau. \quad (2.6)$$

In the equation above the \mathcal{O}_j operators are listed in Table 1[29] and $t^0 = 1$, $t^1 = \tau_3$ denote the 2×2 identity and third Pauli matrix in isospin space, respectively, and the isoscalar and isovector coupling constants c_j^0 and c_j^1 , are related to those to protons and neutrons

$\mathcal{Q}_1^{(5)}$	$\rightarrow -\frac{\alpha}{2\pi} F_1^N \left(\frac{1}{m_\chi} \mathcal{O}_1^N - 4 \frac{m_N}{\bar{q}^2} \mathcal{O}_5^N \right) - \frac{2\alpha}{\pi} \frac{\mu_N}{m_N} \left(\mathcal{O}_4^N - \frac{m_N^2}{\bar{q}^2} \mathcal{O}_6^N \right) + \mathcal{O}(q^2)$
$\mathcal{Q}_2^{(5)}$	$\rightarrow \frac{2\alpha}{\pi} \frac{m_N}{\bar{q}^2} F_1^N \mathcal{O}_{11}^N + \mathcal{O}(q^2)$
$\mathcal{Q}_{1,q}^{(6)}$	$\rightarrow F_1^{q/N} \mathcal{O}_1^N + \mathcal{O}(q^2)$
$\mathcal{Q}_{2,q}^{(6)}$	$\rightarrow 2F_1^{q/N} \mathcal{O}_8^N + 2(F_1^{q/N} + F_2^{q/N}) \mathcal{O}_9^N + \mathcal{O}(q^2)$
$\mathcal{Q}_{3,q}^{(6)}$	$\rightarrow -2F_A^{q/N} \left(\mathcal{O}_7^N - \frac{m_N}{m_\chi} \mathcal{O}_9^N \right) + \mathcal{O}(q^2)$
$\mathcal{Q}_{4,q}^{(6)}$	$\rightarrow -4F_A^{q/N} \mathcal{O}_4^N + F_{P'}^{q/N} \mathcal{O}_6^N + \mathcal{O}(q^2)$
$\mathcal{Q}_1^{(7)}$	$\rightarrow F_G^N \mathcal{O}_1^N + \mathcal{O}(q^2)$
$\mathcal{Q}_2^{(7)}$	$\rightarrow -\frac{m_N}{m_\chi} F_G^N \mathcal{O}_{11}^N + \mathcal{O}(q^3)$
$\mathcal{Q}_3^{(7)}$	$\rightarrow F_G^N \mathcal{O}_{10}^N + \mathcal{O}(q^3)$
$\mathcal{Q}_4^{(7)}$	$\rightarrow \frac{m_N}{m_\chi} F_G^N \mathcal{O}_6^N + \mathcal{O}(q^4)$
$\mathcal{Q}_{5,q}^{(7)}$	$\rightarrow F_S^{q/N} \mathcal{O}_1^N + \mathcal{O}(q)$
$\mathcal{Q}_{6,q}^{(7)}$	$\rightarrow -\frac{m_N}{m_\chi} F_S^{q/N} \mathcal{O}_{11}^N + \mathcal{O}(q^2)$
$\mathcal{Q}_{7,q}^{(7)}$	$\rightarrow F_P^{q/N} \mathcal{O}_{10}^N + \mathcal{O}(q^3)$
$\mathcal{Q}_{8,q}^{(7)}$	$\rightarrow \frac{m_N}{m_\chi} F_P^{q/N} \mathcal{O}_6^N + \mathcal{O}(q^4)$
$\mathcal{Q}_{9,q}^{(7)}$	$\rightarrow 8F_{T,0}^{q/N} \mathcal{O}_4^N + \mathcal{O}(q^2)$
$\mathcal{Q}_{10,q}^{(7)}$	$\rightarrow -2\frac{m_N}{m_\chi} F_{T,0}^{q/N} \mathcal{O}_{10}^N + 2(F_{T,0}^{q/N} - F_{T,1}^{q/N}) \mathcal{O}_{11}^N - 8F_{T,0}^{q/N} \mathcal{O}_{12}^N + \mathcal{O}(q^3)$

Table 2. Correspondence between the relativistic operators listed in Eqs.(2.1–2.3) and the non-relativistic Galilean invariant operators listed in Table 1.

c_j^p and c_j^n by $c_j^p = (c_j^0 + c_j^1)/2$ and $c_j^n = (c_j^0 - c_j^1)/2$. In general, for a given relativistic operator $\mathcal{Q}^{(d)}$ the ensuing coefficients c_j^r may depend on the WIMP mass and/or the exchanged momentum $q \equiv |\vec{q}|$. In Table 2 we summarize such correspondence. We choose for convenience to adopt the same notation used in Ref. [20], and the explicit expression of the low-energy coefficients can be found in the Appendix A of the same paper, or in [6]. In particular, for their numerical calculation we will use the output of the code DirectDM [40].

For the details of the expression to calculate the expected rate in a DD experiment we refer, for instance, to Section 2 of [41]. Once the coefficients of the non-relativistic Hamiltonian in Eq. (2.6) are obtained, for a given recoil energy imparted to the target the differential rate for the WIMP–nucleus scattering process is given by:

$$\frac{dR_{\chi T}}{dE_R}(t) = \sum_T N_T \frac{\rho_{\text{WIMP}}}{m_{\text{WIMP}}} \int_{v_{\min}} d^3 v_T f(\vec{v}_T, t) v_T \frac{d\sigma_T}{dE_R}, \quad (2.7)$$

where ρ_{WIMP} is the local WIMP mass density in the neighborhood of the Sun, N_T the number of the nuclear targets of species T in the detector (the sum over T applies in the

case of more than one target), while

$$\frac{d\sigma_T}{dE_R} = \frac{2m_T}{4\pi v_T^2} \left[\frac{1}{2j_\chi + 1} \frac{1}{2j_T + 1} |\mathcal{M}_T|^2 \right], \quad (2.8)$$

with:

$$\frac{1}{2j_\chi + 1} \frac{1}{2j_T + 1} |\mathcal{M}_T|^2 = \frac{4\pi}{2j_T + 1} \sum_{\tau=0,1} \sum_{\tau'=0,1} \sum_k R_k^{\tau\tau'} \left[c_j^\tau, (v_T^\perp)^2, \frac{q^2}{m_N^2} \right] W_{Tk}^{\tau\tau'}(y). \quad (2.9)$$

In the above expression the squared amplitude $|\mathcal{M}_T|^2$ is summed over initial and final spins, the $R_k^{\tau\tau'}$'s are WIMP response functions which depend on the couplings c_j^τ as well as the transferred momentum \vec{q} , while:

$$(v_T^\perp)^2 = v_T^2 - v_{min}^2, \quad (2.10)$$

and:

$$v_{min}^2 = \frac{q^2}{4\mu_T^2} = \frac{m_T E_R}{2\mu_T^2}, \quad (2.11)$$

represents the minimal incoming WIMP speed required to impart the nuclear recoil energy E_R . Moreover, in equation (2.9) the $W_{Tk}^{\tau\tau'}(y)$'s are nuclear response functions and the index k represents different effective nuclear operators, which, under the assumption that the nuclear ground state is an approximate eigenstate of P and CP , can be at most eight: following the notation in [28, 29], $k=M, \Phi'', \Phi''M, \tilde{\Phi}', \Sigma'', \Sigma', \Delta, \Delta\Sigma'$. The $W_{Tk}^{\tau\tau'}(y)$'s are function of $y \equiv (qb/2)^2$, where b is the size of the nucleus. For the target nuclei T used in most DD experiments the functions $W_{Tk}^{\tau\tau'}(y)$, calculated using nuclear shell models, have been provided in Refs. [29, 42]. Details about the definitions of both the functions $R_k^{\tau\tau'}$'s and $W_{Tk}^{\tau\tau'}(y)$'s can be found in [29]. In particular, W_M corresponds to the standard Spin-Independent (SI) interaction, while $W_{\Sigma''} + W_{\Sigma'}$ (with $W_{\Sigma'} \simeq 2W_{\Sigma''}$) to the standard Spin-Dependent one (SD). Using the decomposition:

$$R_k^{\tau\tau'} = R_{0k}^{\tau\tau'} + R_{1k}^{\tau\tau'} (v_T^\perp)^2 = R_{0k}^{\tau\tau'} + R_{1k}^{\tau\tau'} (v_T^2 - v_{min}^2), \quad (2.12)$$

the correspondence between each term of the Non Relativistic (NR) effective interaction in (2.6) and the $W_{Tk}^{\tau\tau'}(y)$ nuclear response functions is summarized in Table 3.

Finally, $f(\vec{v}_T)$ is the WIMP velocity distribution, for which we assume a standard isotropic Maxwellian at rest in the Galactic rest frame truncated at the escape velocity u_{esc} , and boosted to the Lab frame by the velocity of the Earth. So for the former we assume:

NR coupling	$R_{0k}^{\tau\tau'}$	$R_{1k}^{\tau\tau'}$	coupling	$R_{0k}^{\tau\tau'}$	$R_{1k}^{\tau\tau'}$
1	$M(q^0)$	-	3	$\Phi''(q^4)$	$\Sigma'(q^2)$
4	$\Sigma''(q^0), \Sigma'(q^0)$	-	5	$\Delta(q^4)$	$M(q^2)$
6	$\Sigma''(q^4)$	-	7	-	$\Sigma'(q^0)$
8	$\Delta(q^2)$	$M(q^0)$	9	$\Sigma'(q^2)$	-
10	$\Sigma''(q^2)$	-	11	$M(q^2)$	-
12	$\Phi''(q^2), \tilde{\Phi}'(q^2)$	$\Sigma''(q^0), \Sigma'(q^0)$	13	$\tilde{\Phi}'(q^4)$	$\Sigma''(q^2)$
14	-	$\Sigma'(q^2)$	15	$\Phi''(q^6)$	$\Sigma'(q^4)$

Table 3. Nuclear response functions corresponding to each coupling, for the velocity-independent and the velocity-dependent components parts of the WIMP response function, decomposed as in Eq.(2.12). In parenthesis is the power of $q=|\vec{q}|$ in the WIMP response function.

$$f(\vec{v}_T, t) = \frac{1}{N} \left(\frac{3}{2\pi v_{rms}^2} \right)^{3/2} e^{-\frac{3|\vec{v}_T + \vec{v}_E|^2}{2v_{rms}^2}} \Theta(u_{esc} - |\vec{v}_T + \vec{v}_E(t)|) \quad (2.13)$$

$$N = \left[\text{erf}(z) - \frac{2}{\sqrt{\pi}} z e^{-z^2} \right]^{-1}, \quad (2.14)$$

with $z = 3u_{esc}^2/(2v_{rms}^2)$. In the isothermal sphere model hydrothermal equilibrium between the WIMP gas pressure and gravity is assumed, leading to $v_{rms} = \sqrt{3/2}v_0$ with v_0 the galactic rotational velocity. The yearly modulation effect is due to the time dependence of the Earth's speed with respect to the Galactic frame:

$$|\vec{v}_E(t)| = v_{Sun} + v_{orb} \cos \gamma \cos \left[\frac{2\pi}{T_0}(t - t_0) \right], \quad (2.15)$$

where $\cos \gamma \simeq 0.49$ accounts for the inclination of the ecliptic plane with respect to the Galactic plane, $T_0=1$ year, $t_0=2$ June, $v_{orb}=2\pi r_{\oplus}/(T_0) \simeq 29$ km/sec ($r_{\oplus}=1$ AU, neglecting the small eccentricity of the Earth's orbit around the Sun) while $v_{Sun}=v_0+12$, accounting for a peculiar component of the solar system with respect to the galactic rotation. For the two parameters v_0 and u_{esc} we take $v_0=220$ km/sec [43] and $u_{esc}=550$ km/sec [44]. In the isothermal model the time dependence of Eq. (2.15) induces an expected rate with the functional form $S(t) = S_0 + S_m \cos(2\pi/T - t_0)$, with $S_m > 0$ at large values of v_{min} and turning negative when $v_{min} \lesssim 200$ km/s.

The expected rate in a given visible energy bin $E'_1 \leq E' \leq E'_2$ of a DD experiment is finally given by:

$$R_{[E'_1, E'_2]}(t) = MT_{exp} \int_{E'_1}^{E'_2} \frac{dR}{dE'}(t) dE' \quad (2.16)$$

$$\frac{dR}{dE'}(t) = \sum_T \int_0^\infty \frac{dR_{\chi T}(t)}{dE_{ee}} \mathcal{G}_T(E', E_{ee}) \epsilon(E') dE_{ee} \quad (2.17)$$

$$E_{ee} = Q(E_R)E_R, \quad (2.18)$$

with $\epsilon(E') \leq 1$ the experimental efficiency/acceptance. In the equations above E_R is the recoil energy deposited in the scattering process (indicated in keVnr), while E_{ee} (indicated in keVee) is the fraction of E_R that goes into the experimentally detected process (ionization, scintillation, heat) and $Q(E_R)$ is the quenching factor, $\mathcal{G}_T(E', E_{ee} = Q(E_R)E_R)$ is the probability that the visible energy E' is detected when a WIMP has scattered off an isotope T in the detector target with recoil energy E_R , M is the fiducial mass of the detector and T_{exp} the live-time exposure of the data taking.

In particular, in each visible energy bin DAMA is sensitive to the yearly modulation amplitude S_m , defined as the cosine transform of $R_{[E'_1, E'_2]}(t)$:

$$S_{m, [E'_1, E'_2]} \equiv \frac{2}{T_0} \int_0^{T_0} \cos \left[\frac{2\pi}{T_0}(t - t_0) \right] R_{[E'_1, E'_2]}(t) dt, \quad (2.19)$$

while other experiments put upper bounds on the time average S_0 :

$$S_{0, [E'_1, E'_2]} \equiv \frac{1}{T_0} \int_0^{T_0} R_{[E'_1, E'_2]}(t) dt. \quad (2.20)$$

The expressions above can be recast in the form [45]:

$$S_{m, 0, [E'_1, E'_2]} = \int_0^\infty \mathcal{R}(v) \eta_{m, 0}(v) dv \quad (2.21)$$

with $\mathcal{R}(v)$ a response function which contains the dependence on the particle and nuclear physics while:

$$\eta_0(v) = \frac{1}{T_0} \int_0^{T_0} \eta(v, t) dt, \quad (2.22)$$

$$\eta_m(v) = \frac{2}{T_0} \int_0^{T_0} \cos \left[\frac{2\pi}{T_0}(t - t_0) \right] \eta(v, t) dt, \quad (2.23)$$

$$\eta(v, t) = \int_v^\infty \frac{f(v', t)}{v'} dv', \quad (2.24)$$

are halo functions that contain the dependence on astrophysics.

In the present paper we will systematically consider the possibility that the WIMP–nucleus interaction is driven by one of the effective couplings $\mathcal{C}^{(d)}$ of Eqs. (2.1–2.3).

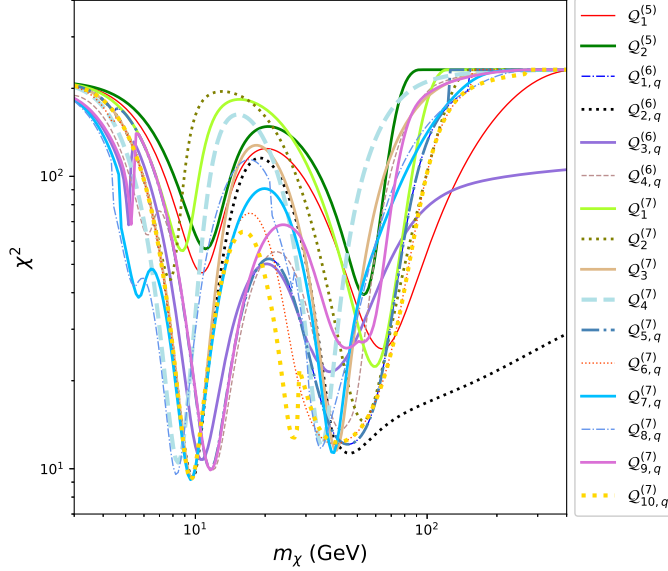


Figure 1. Minimum of the χ^2 of Eq.(3.1) at fixed WIMP mass m_χ as a function of m_χ for each of the different WIMP-nucleus interactions of Eqs. (2.1–2.3).

3 Analysis

The DAMA collaboration has released modulation amplitudes $S_{m,k}^{exp} \equiv S_{m,[E'_k, E'_{k+1}]}$, with uncertainties σ_k , (corresponding to the predictions of Eq.(2.19)) in the visible energy range $1 \text{ keVee} < E' < 20 \text{ keVee}$ in 0.5 keVee energy bins for a total exposure $\simeq 2.46 \text{ ton year}$, corresponding to the combination of DAMA/NaI [46], DAMA/LIBRA–phase1 [47, 48] and DAMA/LIBRA–phase2 [49]. In our analysis we will assume constant quenching factors $Q=0.3$ for sodium, $Q=0.09$ for iodine and a Gaussian energy resolution $\mathcal{G}(E', E_{ee}) = \text{Gauss}(E'|E_{ee}, \sigma) = 1/(\sqrt{2\pi}\sigma)\exp(-(E' - E_{ee})/2\sigma^2)$ with $\sigma = 0.0091 (E_{ee}/\text{keVee}) + 0.448 \sqrt{E_{ee}}/\text{keVee}$ in keVee. To compare the theoretical predictions to the experimental data, for each coupling $\mathcal{C}^{(d)}$ we consider 14 energy bins, of 0.5 keVee width, from 1 keVee to 8 keVee , and one high–energy control bin from 8 keVee to 16 keVee ($[E'_k, E'_{k+1}]$, $k = 1, \dots, 15$). We perform our χ^2 test constructing the quantity:

$$\chi^2(m_\chi, \tilde{\Lambda}, r) = \sum_{k=1}^{15} \frac{[S_{m,k} - S_{m,k}^{exp}(m_\chi, \tilde{\Lambda}, r)]^2}{\sigma_k^2}, \quad (3.1)$$

and minimize it as a function of $(m_\chi, \tilde{\Lambda}, r)$ (WIMP–photon and WIMP–gluon interactions do not depend on the r parameter).

Q	$m_{\chi,\min}$ (GeV)	$r_{\chi,\min}$	$\tilde{\Lambda}_{\min}$ (GeV)	χ^2_{\min}
$Q_1^{(5)}$	63.95	–	121.44	25.70
	10.62	–	101.16	46.74
$Q_2^{(5)}$	53.29	–	50770.1	39.36
	11.09	–	49155.7	56.45
$Q_{1,q}^{(6)}$	11.62	-0.88	311.62	9.94
	45.55	-0.87	516.67	12.11
$Q_{2,q}^{(6)}$	9.71	-1.14	29.55	9.28
	46.24	-0.58	82.53	11.28
$Q_{3,q}^{(6)}$	10.65	3.30	2.20	10.70
	38.13	-5.43	8.06	21.45
$Q_{4,q}^{(6)}$	11.93	3.17	62.68	9.90
	42.43	2.93	82.26	13.58
$Q_1^{(7)}$	59.46	–	60.50	22.32
	8.77	–	35.92	55.54
$Q_2^{(7)}$	53.02	–	5.73	14.58
	7.74	–	3.60	44.08
$Q_3^{(7)}$	9.63	–	3.80	9.26
	40.42	–	6.96	11.53
$Q_{4,q}^{(7)}$	8.40	–	0.384	10.49
	35.05	–	0.712	11.93
$Q_{5,q}^{(7)}$	11.62	-0.20	5.26	9.94
	45.55	-0.20	7.38	12.11
$Q_{6,q}^{(7)}$	9.57	-0.20	1.12	9.16
	40.12	-0.20	2.64	12.16
$Q_{7,q}^{(7)}$	9.56	0.40	2.24	9.16
	39.20	0.39	4.22	11.26
$Q_{8,q}^{(7)}$	8.27	0.36	0.366	9.52
	34.71	0.14	1.44	11.70
$Q_{9,q}^{(7)}$	11.66	4.81	3.73	9.88
	44.94	3.65	3.77	25.84
$Q_{10,q}^{(7)}$	9.57	-0.35	2.13	9.16
	40.78	-0.32	6.59	12.30

Table 4. Absolute and local minima of the χ^2 defined in Eq.(3.1) for each of the relativistic models $Q_{a,q}^{(d)}$ and $Q_b^{(d)}$ of Eqs. (2.1–2.3).

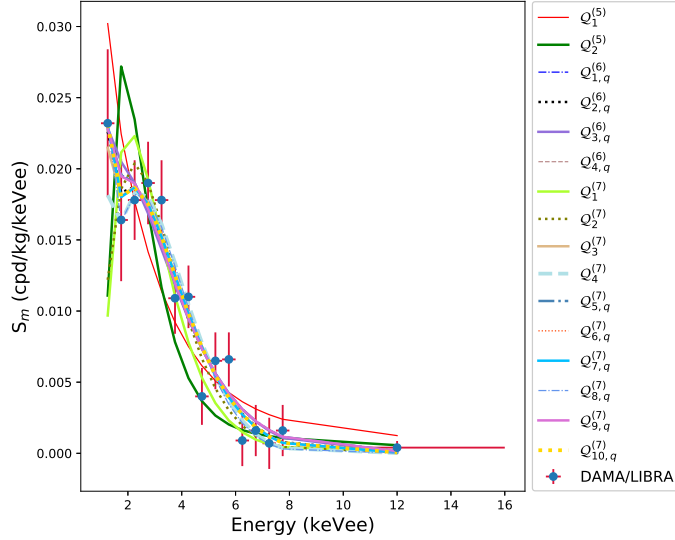


Figure 2. DAMA modulation amplitudes as a function of the measured ionization energy E_{ee} for the absolute minima of Table 4 for each of the effective models of Eqs. (2.1–2.3). The points with error bars correspond to the combined data of DAMA/NaI [46], DAMA/LIBRA–phase1 [47, 48] and DAMA/LIBRA–phase2 [49].

In Fig. 1 we show the result of such minimization at fixed WIMP mass m_χ . From such figure one can see that for each coupling $\mathcal{C}^{(d)}$ two local minima are obtained. The details of such minima are provided in Table 4, and the ensuing predictions for the modulation amplitudes in the absolute minima of each model are compared to those measured by DAMA in Fig 2. Moreover, the contour plots of $\chi^2 - \chi_{min}^2 = n^2$ with $n = 5$ (5σ regions) in the $m_\chi - \tilde{\Lambda}$ plane (minimized with respect to the r parameter introduced in Eq. (2.5), when applicable) are also provided in Fig. 3 for each of the 13 WIMP-nucleus interactions that yield an acceptable χ^2 in the absolute minimum (in the following discussion we refer to a good fit when the p -value is larger than 0.05, i.e. $\chi^2 \lesssim 21$ for 15-3 d.o.f. and $\chi^2 \lesssim 22$ for 15-2 d.o.f.). In the same figure the stars correspond to the absolute minima of Table 4.

The results summarized in Table 4 can be understood in terms of a combination of kinematics, mainly driven by the cosine transform of the halo function defined in Eq. (2.23), and dynamics, determined instead by the correspondence between each relativistic model coupling and its non-relativistic limit, as summarized in Table 2.

To illustrate the role of the halo function in the kinematics of the scattering process, in Fig. 4 we plot the function $\eta_m(v)$. In particular, if in Eq. (2.21) the response function \mathcal{R} does not show a strong energy dependence induced by the nuclear form factor, or, as in the case of the \mathcal{O}_7 or \mathcal{O}_{14} NR operators, an explicit dependence on the velocity v

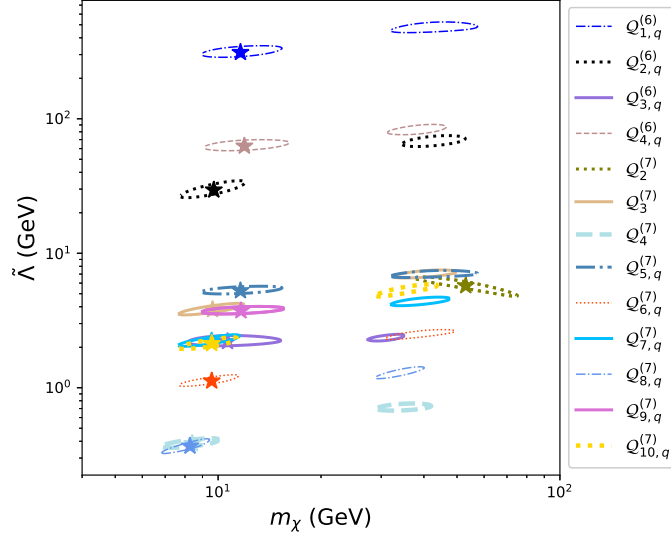


Figure 3. Contour plots of $\chi^2 - \chi_{min}^2 = n^2$ with $n = 5$ (5σ regions) in the $m_\chi - \tilde{m}$ plane (minimized with respect to the r parameter introduced in Eq. (2.5), when applicable) for each of the 13 WIMP-nucleus interactions that yield an acceptable χ^2 . The stars correspond to the absolute minima of Table 4.

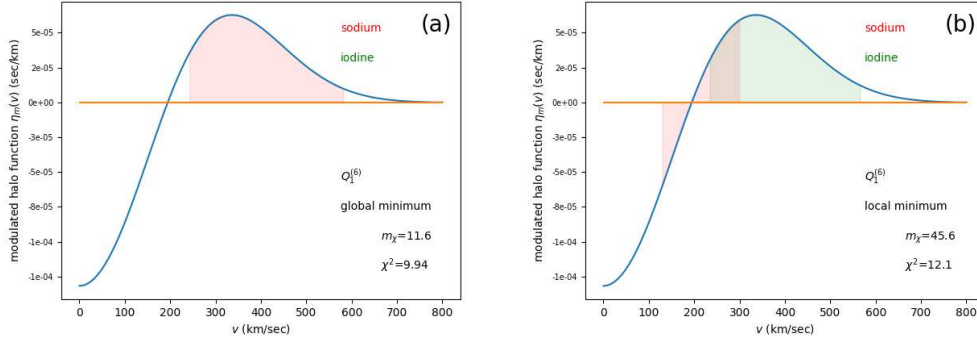


Figure 4. Cosine transform η_m of the halo function $\eta(v, t)$ defined in Eq. 2.23, and entering the expected amplitudes parameterization of Eq. 2.21. In the same figures the shaded areas represent the range of v contributing to the DAMA modulated amplitudes between 1 keVee and 6 keVee for WIMP-sodium scattering (red) and WIMP-iodine scattering (green) for the interaction term $Q_{1,q}^{(6)}$ and in the minima of Table 4. (a): low-mass minimum; (b): high-mass minimum.

through a non-vanishing $R_{1k}^{\tau\tau'}$ (see Eq. (2.12)) it is the $\eta_m(v)$ halo function that drives the energetic spectral shape of the modulation amplitude, and the latter can well reproduce the maximum observed above 2 keVee (see Fig. 2), once the v range close to $\simeq 340$ km/sec (for our choice of astrophysical parameters) is mapped to recoil energies around $\simeq 3$ keVee through Eq. (2.11). Indeed, with a few exceptions discussed below, this is the mechanism that allows to achieve most of the acceptable χ^2 's listed in Table 4. However, due to the different kinematics of the two processes, the energy range of the observed maximum corresponds to two different values of m_χ for WIMP-sodium and WIMP-iodine scattering. This explains the systematic presence of two minima in the χ^2 .

Moreover, in Fig. 4 the shaded areas represent the range of v contributing to the DAMA modulated amplitudes between 1 keVee and 6 keVee for WIMP-sodium scattering (red) and WIMP-iodine scattering (green) in the specific example of the interaction term $\mathcal{Q}_{1,q}^{(6)}$ and in the corresponding two minima of Table 4 (such v ranges are defined as the intervals where in Eq. (2.21) the response function $\mathcal{R}(v)$ is different from zero). In particular, in Fig. 4(a), where the shaded areas are shown for the low-mass minimum, one can see that scattering off iodine is driven to v values very close to the escape velocity (for this reason it is not visible). Indeed, in such case scattering off iodine is kinematically accessible only below 2 keVee, while above that energy sodium alone contributes to the expected signal. On the other hand, Fig. 4(b) shows that in the high-mass minimum both targets contribute. However, in this case sodium is pushed down to low v values, where the modulation amplitude is suppressed.

As a consequence of the above discussion, the goodness-of-fit of the DAMA modulation amplitudes at low WIMP mass is sensitive to both WIMP-iodine and WIMP-sodium scattering, and so to the scaling between the two corresponding cross sections [23, 50, 51]. Indeed, in such case, provided that such hierarchy is not too large, a good fit can be attained since the energy dependence of the modulation amplitude is mostly driven by the $\eta_m(v)$ halo function and is only slightly modified above 2 keVee by the sodium form factor, which has a mild additional energy dependence due to the small size target and the sensitivity to smaller recoil energies at fixed electron-equivalent ones compared to iodine due to the larger quenching factor. On top of that, below 2 keVee WIMP-iodine scattering can provide a nice fit to the modulation amplitude measured by DAMA in the first energy bin: indeed, it is for this reason that in Table 4 most of the absolute minima correspond to the low WIMP mass solution. Among the different NR operators of Table 1 the case of a standard SI cross section, which corresponds to the NR operator \mathcal{O}_1 , shows the largest hierarchy between the WIMP-iodine and WIMP-sodium cross sections, since they depend on the nuclear response function $W_M^{\tau\tau'}$ (see Table 3) which scales with the mass numbers of the two targets. This makes it hard to fit WIMP-sodium scattering above 2 keVee without overestimating the WIMP-iodine process at lower energy unless the non-relativistic couplings c_j^n/c_j^p off neutrons and protons are tuned to suppress the WIMP-iodine cross section, as pointed out in [23, 50, 52]. In particular, by combining the information contained in

Table 2 and Table 3 one can notice that nine out of the sixteen relativistic effective models of Table 4 take contribution from the $W_{TM}^{\tau\tau'}$ nuclear response function: $\mathcal{Q}_1^{(5)}$, $\mathcal{Q}_2^{(5)}$, $\mathcal{Q}_1^{(6)}$, $\mathcal{Q}_1^{(6)}$, $\mathcal{Q}_1^{(7)}$, $\mathcal{Q}_2^{(7)}$, $\mathcal{Q}_{5,q}^{(7)}$, $\mathcal{Q}_{6,q}^{(7)}$ and $\mathcal{Q}_{10,q}^{(7)}$. In particular, four of such operators correspond to effective interactions between the WIMP and gauge bosons (the photon and the gluon) for which the ratio between the non-relativistic couplings c_j^n/c_j^p is fixed, and cannot be tuned to reduce the χ^2 : $\mathcal{Q}_1^{(5)}$, $\mathcal{Q}_2^{(5)}$, $\mathcal{Q}_1^{(7)}$ and $\mathcal{Q}_2^{(7)}$. Indeed, at low WIMP mass model $\mathcal{Q}_1^{(7)}$ has $\chi^2=22.32$ and $\mathcal{Q}_2^{(7)}$ has $\chi^2=44.08$, while the χ^2 for models $\mathcal{Q}_1^{(5)}$ and $\mathcal{Q}_2^{(5)}$ is even higher, since they have the additional feature that the $1/q^2$ propagator further enhances the expected modulation amplitudes in the first two energy bins (for such long-range interactions this implies that also the χ^2 at large WIMP masses is not acceptable). On the other hand the interactions $\mathcal{Q}_{1,q}^{(6)}$, $\mathcal{Q}_{2,q}^{(6)}$, $\mathcal{Q}_{5,q}^{(7)}$, $\mathcal{Q}_{6,q}^{(7)}$ and $\mathcal{Q}_{10,q}^{(7)}$ allow to tune the r parameter to suppress the iodine contribution, leading to an acceptable χ^2 . Finally, the remaining seven interactions $\mathcal{Q}_3^{(6)}$, $\mathcal{Q}_4^{(6)}$, $\mathcal{Q}_3^{(7)}$, $\mathcal{Q}_4^{(7)}$, $\mathcal{Q}_7^{(7)}$, $\mathcal{Q}_8^{(7)}$ and $\mathcal{Q}_9^{(7)}$ achieve a good χ^2 at small m_χ without any particular tuning because they are all driven by SD type nuclear form factors (i.e. $W_{T\Sigma''}^{\tau\tau'}$ and/or $W_{T\Sigma'}^{\tau\tau'}$) for which no large hierarchy is observed in the first place between the WIMP–iodine and the WIMP–sodium cross sections.

As far as the large-mass minima of Table 4 are concerned, as explained above they correspond to the situation when WIMP–iodine scattering maps the maximum of the halo function $\eta_m(v)$ at $v \simeq 340$ km/sec to recoil energies $\simeq 3$ keV. In this case to get an acceptable fit the WIMP–sodium scattering process is not relevant, since, as shown in Fig. 4(b), for such WIMP masses it is driven to values of v where its contribution to the modulation is suppressed. As a consequence, in the high-mass minima the modulation amplitudes are sensitive to WIMP–iodine scattering alone, while the hierarchy between the WIMP–sodium and WIMP–iodine cross sections does not play a significant role. In this case, however, another effect kicks in: due to the large size and the small quenching of the iodine target all the corresponding nuclear form factors $W_{T_k}^{\tau\tau'}$ show a much steeper energy dependence compared to that of sodium. This additional energy dependence in the WIMP response function \mathcal{R} alters the spectrum provided by the $\eta_m(v)$ halo function alone spoiling the goodness-of-fit at large WIMP masses, unless some mechanism is active to reduce it. In the models where an acceptable χ^2 is achieved at large WIMP mass this mechanism is provided by an explicit momentum suppression in the WIMP response function $R_k^{\tau\tau'}$ and/or (in the case of WIMP–quark interactions driven by $W_{TM}^{\tau\tau'}$) by a tuning of the c^n/c^p ratio.

In particular this explains why, out of the seven models with a momentum-suppressed SD type interaction ($\mathcal{Q}_{3,q}^{(6)}$ and $\mathcal{Q}_{9,q}^{(7)}$, $\mathcal{Q}_{4,q}^{(6)}$, $\mathcal{Q}_3^{(7)}$, $\mathcal{Q}_4^{(7)}$, $\mathcal{Q}_{7,q}^{(7)}$ and $\mathcal{Q}_{8,q}^{(7)}$) all achieve a good χ^2 at large WIMP masses with the exception of $\mathcal{Q}_{3,q}^{(6)}$ and $\mathcal{Q}_{9,q}^{(7)}$. It is worth noting that this implies that for $\mathcal{Q}_{4,q}^{(6)}$ a tuning of the r parameter to enhance the \mathcal{O}_6 contribution (q^4 suppressed) compared to \mathcal{O}_4 (with no momentum suppression) is required to achieve a good χ^2 . Indeed, the \mathcal{O}_4 operator (i.e. a standard, SD interaction) has already been shown to yield a bad

fit at large m_χ to the DAMA data [23]. This also explains why $\mathcal{Q}_{9,q}^{(7)}$, that corresponds to the NR operator \mathcal{O}_4 alone (again, see Table 2) yields a bad χ^2 . On the other hand, the operator $\mathcal{Q}_{3,q}^{(6)}$ corresponds to a combination of \mathcal{O}_7 and \mathcal{O}_9 , with the latter suppressed at large m_χ (see Table 2) so that in this case the contribution of \mathcal{O}_7 turn out to be sizeable. However (see Table 3 and Eq. (2.12)) the WIMP response function $R_k^{\tau\tau'}$ of \mathcal{O}_7 shows in this case an explicit dependence on v^2 that spoils the fit (the same was observed in the fit of the \mathcal{O}_7 operator of Ref. [23]). For the five models that depend on $W_{TM}^{\tau\tau'}$ and that correspond to effective interactions of the WIMP to quarks ($\mathcal{Q}_{1,q}^{(6)}$, $\mathcal{Q}_{2,q}^{(6)}$, $\mathcal{Q}_{5,q}^{(7)}$, $\mathcal{Q}_{6,q}^{(7)}$ and $\mathcal{Q}_{10,q}^{(7)}$) besides momentum suppression, when present, the ratio of the non-relativistic couplings c_j^n/c_j^p can be tuned to reduce the steepness of the iodine SI form factor and achieve an acceptable χ^2 . Such dependence on c^n/c^p is not present for the two WIMP–gluon effective interactions $\mathcal{Q}_{1,q}^{(7)}$ and $\mathcal{Q}_{2,q}^{(7)}$: the former has no momentum suppression either, and so yields a bad χ^2 , while the latter is momentum suppressed, so corresponds to an acceptable goodness-of-fit.

The axial current in $\mathcal{Q}_{4,q}^{(6)}$, the pseudoscalar current in $\mathcal{Q}_{7,q}^{(7)}$ and $\mathcal{Q}_{8,q}^{(7)}$ and the CP-odd gluonic current in $\mathcal{Q}_{3,q}^{(7)}$ and $\mathcal{Q}_{4,q}^{(7)}$ deserve a few additional comments since they receive contributions from light pseudoscalar meson exchanges [20] that can potentially modify the modulation energy spectrum. In particular, this implies that the Wilson coefficients of the NR effective theory can potentially acquire an additional momentum dependence, since in Table 2 one has [20]:

$$F_{P,P'}^{q/N}(q^2) = \frac{m_N^2}{m_\pi^2 + q^2} a_\pi^{q/N} + \frac{m_N^2}{m_\eta^2 + q^2} a_\eta^{q/N} + b^{q/N}, \quad (3.2)$$

$$F_{\tilde{G}}^N(q^2) = \frac{-q^2}{m_\pi^2 + q^2} a_{\tilde{G},\pi}^N + \frac{-q^2}{m_\eta^2 + q^2} a_{\tilde{G},\eta}^N + b_{\tilde{G}}^N, \quad (3.3)$$

with $m_\pi \simeq 135$ MeV and $m_\eta \simeq 547$ MeV the pion and eta meson masses, and $a_\pi^{q/N}$, $a_\eta^{q/N}$, $b^{q/N}$, $a_{\tilde{G},\pi}^N$, $a_{\tilde{G},\eta}^N$ and $b_{\tilde{G}}^N$ constants that we calculate using the code DirectDM [40] and that depend on the r parameter. In particular, in light of the previous discussion such meson propagators, as in the case of the long-range interactions $\mathcal{Q}_1^{(5)}$ and $\mathcal{Q}_2^{(5)}$, could potentially spoil the fit to the DAMA modulation amplitudes. However, what we observe is that the effect of such poles is always mild. In fact one should first notice that meson poles can modify the energy spectrum only for a pion propagator, and only when the scattering rate is driven by WIMP–iodine scattering, since in this case one has $q^2 = 2M_T E_R \lesssim 0.8 m_\pi^2$ in the DAMA signal region $E_{ee} \lesssim 6$ keVee (the same quantity for sodium is $q^2 \lesssim 0.04 m_\pi^2$). Moreover, in the case of the CP-odd gluonic current of $\mathcal{Q}_{3,q}^{(7)}$ and $\mathcal{Q}_{4,q}^{(7)}$ the constant term $b_{\tilde{G}}^N$ is LO and dominates the Wilson coefficient, with the poles representing a small correction, as we observe numerically. Also, in the case of $\mathcal{Q}_{4,q}^{(6)}$ the contribution of the term $F_{P'}\mathcal{O}_6$, albeit, as pointed out previously, instrumental to improve the fit at high WIMP mass, does not

exceed $\simeq 10\%$ of the total rate. Only in the case of the pseudoscalar current in $\mathcal{Q}_{7,q}^{(7)}$ and $\mathcal{Q}_{8,q}^{(7)}$ the constant term $b^{q/N}$ is NLO, so in this case the terms proportional to the meson poles actually drive the predicted rates. However both in $\mathcal{Q}_{7,q}^{(7)}$ and $\mathcal{Q}_{8,q}^{(7)}$ after hadronization [20] the pion pole acquires an isovector coupling ($c_\pi^p \simeq -c_\pi^n$) and the eta pole an isoscalar one ($c_\eta^p \simeq c_\eta^n$) so that $F_{P,P'}^{q/N} \rightarrow c^\tau = c_\pi^1/(m_\pi^2 + q^2) + c_\eta^0/(m_\eta^2 + q^2)$. Taking into account Tables 2 and 3 one can see that in this case the scattering amplitude is proportional to $q^n c^\tau c^{\tau'} W_{T\Sigma''}^{\tau\tau'}$ = $q^n [(c_\pi^1)^2 W_{T\Sigma''}^{11}/(m_\pi^2 + q^2)^2 + 2c_\pi^0 c_\pi^1 W_{T\Sigma''}^{01}/((m_\pi^2 + q^2)(m_\eta^2 + q^2)) + (c_\eta^0)^2 W_{T\Sigma''}^{00}/(m_\eta^2 + q^2)^2]$, with $n=2$ for $\mathcal{Q}_{7,q}^{(7)}$ and $n=4$ for $\mathcal{Q}_{8,q}^{(7)}$. Such expression turns out to have a mild momentum dependence because the three functions $W_{T\Sigma''}^{11}(q)$, $W_{T\Sigma''}^{01}(q)$ and $W_{T\Sigma''}^{00}(q)$ show an increasing steepness in their q dependence that compensates the decreasing steepness of the corresponding pole combinations $1/(m_\pi^2 + q^2)^2$, $1/((m_\pi^2 - q^2)(m_\eta^2 + q^2))$ and $1/(m_\eta^2 + q^2)^2$. The bottom line is that also in this case the overall momentum dependence does not depart significantly from the other momentum-suppressed SD interactions already discussed before, and so a good fit to the DAMA data can be achieved.

Besides the goodness of fit, one should notice at this stage that the values of $\tilde{\Lambda}_{min}$ in Table 4 should be checked for their consistency with the validity of the effective theory. A criterion for the validity of the EFT is to interpret both scales $\tilde{\Lambda}_{up} = \tilde{\Lambda}$ and $\tilde{\Lambda}_{down} \equiv (\mathcal{C}_{down}^{(d)})^{-\frac{1}{d-4}} = \tilde{\Lambda}_{up} \times r^{-\frac{1}{d-4}}$ in terms of the propagator g^2/M_*^2 with $g < \sqrt{4\pi}$ and $M_* > \mu_{scale}$, where, in our analysis, we have fixed the boundary conditions of the EFT at the scale $\mu_{scale} = 2$ GeV. This is straightforward for dimension-6 operators, while in the case of operators whose effective coupling has dimension different from -2 only matching the EFT with the full theory would allow to draw robust conclusions. In particular, in this case $\tilde{\Lambda}_{up}$ and $\tilde{\Lambda}_{down}$ can be interpreted in terms of the same propagator times the appropriate power of a typical scale of the problem μ'_{scale} , which depends on the ultraviolet completion of the EFT. To fix an order of magnitude we choose to fix $\mu'_{scale} = \mu_{scale}$, so that the bound $min(\tilde{\Lambda}_{up}, \tilde{\Lambda}_{down}) > \mu_{scale}/(4\pi)^{1/(d-4)}$ can be derived. Using the values of $\tilde{\Lambda}_{min}$ and r_{min} in Table 4 we obtain that such bound is violated for the global minima of $\mathcal{Q}_4^{(7)}$ and $\mathcal{Q}_{8,q}^{(7)}$ and the local minimum of $\mathcal{Q}_4^{(7)}$. However we stress again that for operators with dimension different from 6 this can only be assessed when a specific ultraviolet completion of the effective theory is assumed.

We conclude this section comparing in Fig. 5 the best-fit values $\tilde{\Lambda}_{min}$ from Table 4 for the effective scale $\tilde{\Lambda}$ and the corresponding experimental lower bound $\tilde{\Lambda}_{limit}$ from XENON1T [53] (Fig. 5(a)) and PICO-60 [54] (Fig. 5(b)). In particular, for XENON1T we have assumed 7 WIMP candidate events in the range of $3PE \leq S_1 \leq 70PE$, as shown in Fig. 3 of Ref. [53] for the primary scintillation signal S1 (directly in Photo Electrons, PE), with an exposure of 278.8 days and a fiducial volume of 1.3 ton of xenon. We have used the efficiency taken from Fig. 1 of [53] and employed a light collection efficiency $g_1=0.055$; for the light yield L_y we have extracted the best estimation curve with an electric field of 90 V/cm from Fig. 7 for Ref. [55]. Moreover, we have modeled the energy resolution

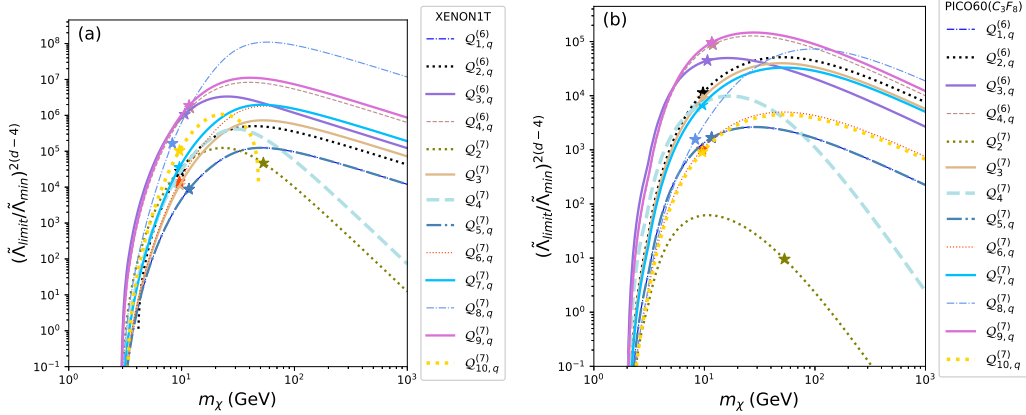


Figure 5. Ratio $(\tilde{\Lambda}_{limit}/\tilde{\Lambda}_{min})^{2(d-4)}$ (with d the dimensionality of the operator) between the experimental lower bound $\tilde{\Lambda}_{limit}$ on the effective scale $\tilde{\Lambda}$ and its best-fit value $\tilde{\Lambda}_{min}$ from Table 4 as a function of the WIMP mass m_χ for each of the 13 relativistic effective models that yield an acceptable χ^2 . Such combination corresponds for each model to the ratio between the expected number of events and the corresponding upper bound. (a) $\tilde{\Lambda}_{min}$ from XENON1T [53]; (b) $\tilde{\Lambda}_{min}$ from PICO-60 [54]. For all models the ratio $r = C_{down}^{(d)}/C_{up}^{(d)}$ is fixed to its best-fit value from Table 4, and the stars indicate the corresponding best-fit value of the WIMP mass m_χ .

combining a Poisson fluctuation of the observed primary signal S_1 compared to $\langle S_1 \rangle = g_1 L_y E_R$ and a Gaussian response of the photomultiplier with $\sigma_{PMT} = 0.5$ [56]. On the other hand, for PICO-60 we have combined the two runs obtained using a C_3F_8 [54] target discussed in [54]: a 1404 kg day exposure and threshold $E_{th}=2.45$, with 3 observed candidate events and 1 event from the expected background, implying an upper bound of 6.42 events at 90% C.L.; a 1167 kg day exposure and threshold $E_{th}=3.3$ keV, with zero observed candidate events and negligible expected background, implying a 90% C.L. upper bound of 2.3 events. For both runs we have assumed the nucleation probabilities in Fig. 3 of [54].

The result of the comparison between the best-fit minima of Table 4 and the XENON1T and PICO-60 constraints is shown in Fig. 5 for each of the 13 models that yield an acceptable χ^2 . In particular, in that figure we plot the combination $(\tilde{\Lambda}_{limit}/\tilde{\Lambda}_{min})^{2(d-4)}$ (with d the dimensionality of the operator) which corresponds to the ratio between the expected number of events and the corresponding upper bound. In both plots the ratio $r = C_{down}^{(d)}/C_{up}^{(d)}$ is fixed to its best-fit value from Table 4 (when applicable), and the stars indicate the corresponding best-fit value of the WIMP mass m_χ . From Fig. (5) one can see that for all the absolute minima of Table 4 the corresponding predicted number of events exceeds by more than three orders of magnitude the upper bound from XENON1T and/or PICO-60.

4 Conclusions

Model-independent approaches have become increasingly popular to interpret Dark Matter search experiments, due to the lack of evidence of any physics beyond the standard model from the LHC. However, in spite of its potential relevance, a completely model-independent assessment of the DAMA modulation result is still not available after almost twenty years of its appearance. In particular, no DAMA analysis in terms of a WIMP effective interaction with photons, gluons and quarks was available so far, and, while the existing ones in terms of the non-relativistic operators allowed by Galilean invariance do not include Wilson coefficients with an explicit momentum dependence, relativistic effective models can induce them. In order to fill this gap in the present paper we have analyzed the DAMA/Libra-phase2 modulation result using a basis of 16 effective operators describing the WIMP interaction with photons, gluons and quarks up to mass dimension seven. For each operator we have fixed the effective theory at the scale of 2 GeV and parameterized the WIMP-quark interaction in terms of two independent couplings $\mathcal{C}_{down}^{(d)}$ and $\mathcal{C}_{up}^{(d)}$ common to up-type and down-type quarks. We have then discussed the fit to the DAMA-phase2 data in terms of the WIMP mass m_χ , the effective scale $\tilde{\Lambda}$ defined through the parameterization $\mathcal{C}_{up}^{(d)}=1/\tilde{\Lambda}^{d-4}$ (with d the effective operator dimensionality) and the ratio $r = \mathcal{C}_{down}^{(d)}/\mathcal{C}_{up}^{(d)}$. For all the effective operators that we considered we obtained two minima, one at low WIMP mass $\simeq 10$ GeV and the other for $m_\chi \gtrsim 35$ GeV. In particular, only nine out of the ensuing thirty-two minima and three out of the sixteen models do not have an acceptable goodness-of-fit. Two additional models ($\mathcal{Q}_4^{(7)}$ and $\mathcal{Q}_{8,q}^{(7)}$) require values of the effective scale below 2 GeV, i.e. the value that we use to fix the Wilson parameters.

In both the low and high m_χ minima for $\mathcal{Q}_1^{(5)}$ and $\mathcal{Q}_2^{(5)}$ (corresponding to a magnetic dipole and electric dipole WIMP coupling) the photon propagator induces a steep rise of the modulation amplitudes at low WIMP recoil energy incompatible to the measured ones for both low and high WIMP masses. In the remaining two models with a bad χ^2 at low m_χ the hierarchy between the WIMP-iodine and the WIMP-sodium cross section is too large because it is of the SI type (i.e. it scales with the atomic squared mass) and cannot be reduced by tuning the r parameter ($\mathcal{Q}_1^{(7)}$ and $\mathcal{Q}_2^{(7)}$). On the other hand, at high m_χ the iodine nuclear form factor has a too steep energy dependence for $\mathcal{Q}_1^{(7)}$ and $\mathcal{Q}_{9,q}^{(7)}$, while model $\mathcal{Q}_{3,q}^{(6)}$ does not yield an acceptable fit because the corresponding WIMP response function depends explicitly on the velocity v . In all the other twenty-three minima a good χ^2 can be achieved. In particular in the twelve low-WIMP mass minima the hierarchy between the WIMP-iodine and the WIMP-sodium cross section is either naturally of order one because of a SD type interaction ($\mathcal{Q}_3^{(6)}$, $\mathcal{Q}_4^{(6)}$, $\mathcal{Q}_3^{(7)}$, $\mathcal{Q}_4^{(7)}$, $\mathcal{Q}_7^{(7)}$, $\mathcal{Q}_8^{(7)}$ and $\mathcal{Q}_9^{(7)}$) or can be kept under control by tuning the r parameter ($\mathcal{Q}_{1,q}^{(6)}$, $\mathcal{Q}_{2,q}^{(6)}$, $\mathcal{Q}_{5,q}^{(7)}$, $\mathcal{Q}_{6,q}^{(7)}$ and $\mathcal{Q}_{10,q}^{(7)}$). Finally, in the eleven large- m_χ minima an acceptable goodness-of-fit is achieved because the steepness of the iodine nuclear form factor is either compensated by an explicit momentum suppression in

the WIMP response function ($\mathcal{Q}_2^{(7)}, \mathcal{Q}_3^{(7)}, \mathcal{Q}_4^{(7)}$) or the steepness of the iodine form factor can be mitigated by tuning the r parameter ($\mathcal{Q}_{1,q}^{(6)}, \mathcal{Q}_{2,q}^{(6)}, \mathcal{Q}_{5,q}^{(7)}, \mathcal{Q}_{6,q}^{(7)}$), or both ($\mathcal{Q}_{4,q}^{(6)}, \mathcal{Q}_{7,q}^{(7)}, \mathcal{Q}_{8,q}^{(7)}$ and $\mathcal{Q}_{10,q}^{(7)}$). Such mechanism is not altered by the effect of the meson poles arising in the axial current of $\mathcal{Q}_{4,q}^{(6)}$, the pseudoscalar current of $\mathcal{Q}_{7,q}^{(7)}$ and $\mathcal{Q}_{8,q}^{(7)}$ and the CP-odd gluonic current of $\mathcal{Q}_{3,q}^{(7)}$ and $\mathcal{Q}_{4,q}^{(7)}$, since they always induce a mild momentum dependence in the scattering amplitude.

For all the minima the corresponding predicted number of events exceeds by more than three orders of magnitude the upper bounds from XENON1T and/or PICO-60.

Acknowledgements

This research was supported through the Basic Science Research Program of the National Research Foundation of Korea (NRF) funded by the Ministry of Education, grant number 2016R1D1A1A09917964 and by the Ministry of Science and ICT, grant number 2019R1F1A1052231.

References

- [1] S. Chang, A. Pierce, and N. Weiner, *Momentum Dependent Dark Matter Scattering*, *JCAP* **1001** (2010) 006, [[arXiv:0908.3192](#)].
- [2] B. A. Dobrescu and I. Mocioiu, *Spin-dependent macroscopic forces from new particle exchange*, *JHEP* **11** (2006) 005, [[hep-ph/0605342](#)].
- [3] J. Fan, M. Reece, and L.-T. Wang, *Non-relativistic effective theory of dark matter direct detection*, *JCAP* **1011** (2010) 042, [[arXiv:1008.1591](#)].
- [4] R. J. Hill and M. P. Solon, *WIMP-nucleon scattering with heavy WIMP effective theory*, *Phys. Rev. Lett.* **112** (2014) 211602, [[arXiv:1309.4092](#)].
- [5] V. Gluscevic and A. H. G. Peter, *Understanding WIMP-baryon interactions with direct detection: A Roadmap*, *JCAP* **1409** (2014), no. 09 040, [[arXiv:1406.7008](#)].
- [6] M. Cirelli, E. Del Nobile, and P. Panci, *Tools for model-independent bounds in direct dark matter searches*, *JCAP* **1310** (2013) 019, [[arXiv:1307.5955](#)].
- [7] S. Chang, R. Edezhath, J. Hutchinson, and M. Luty, *Effective WIMPs*, *Phys. Rev.* **D89** (2014), no. 1 015011, [[arXiv:1307.8120](#)].
- [8] R. Catena, *Prospects for direct detection of dark matter in an effective theory approach*, *JCAP* **1407** (2014) 055, [[arXiv:1406.0524](#)].
- [9] R. Catena, *Dark matter directional detection in non-relativistic effective theories*, *JCAP* **1507** (2015), no. 07 026, [[arXiv:1505.06441](#)].
- [10] R. Catena and P. Gondolo, *Global fits of the dark matter-nucleon effective interactions*, *JCAP* **1409** (2014), no. 09 045, [[arXiv:1405.2637](#)].

- [11] **SuperCDMS** Collaboration, K. Schneck et al., *Dark matter effective field theory scattering in direct detection experiments*, *Phys. Rev.* **D91** (2015), no. 9 092004, [[arXiv:1503.03379](#)].
- [12] R. Catena and P. Gondolo, *Global limits and interference patterns in dark matter direct detection*, *JCAP* **1508** (2015), no. 08 022, [[arXiv:1504.06554](#)].
- [13] H. Rogers, D. G. Cerdeno, P. Cushman, F. Livet, and V. Mandic, *Multidimensional effective field theory analysis for direct detection of dark matter*, *Phys. Rev.* **D95** (2017), no. 8 082003, [[arXiv:1612.09038](#)].
- [14] **XENON** Collaboration, E. Aprile et al., *Effective field theory search for high-energy nuclear recoils using the XENON100 dark matter detector*, *Phys. Rev.* **D96** (2017), no. 4 042004, [[arXiv:1705.02614](#)].
- [15] **CRESST** Collaboration, G. Angloher et al., *Limits on Dark Matter Effective Field Theory Parameters with CRESST-II*, *Eur. Phys. J.* **C79** (2019), no. 1 43, [[arXiv:1809.03753](#)].
- [16] R. J. Hill and M. P. Solon, *Universal behavior in the scattering of heavy, weakly interacting dark matter on nuclear targets*, *Phys. Lett.* **B707** (2012) 539–545, [[arXiv:1111.0016](#)].
- [17] R. J. Hill and M. P. Solon, *Universal behavior in the scattering of heavy, weakly interacting dark matter on nuclear targets*, *Phys. Lett.* **B707** (2012) 539–545, [[arXiv:1111.0016](#)].
- [18] M. Hoferichter, P. Klos, and A. Schwenk, *Chiral power counting of one- and two-body currents in direct detection of dark matter*, *Phys. Lett.* **B746** (2015) 410–416, [[arXiv:1503.04811](#)].
- [19] M. Hoferichter, P. Klos, J. Menéndez, and A. Schwenk, *Analysis strategies for general spin-independent WIMP-nucleus scattering*, *Phys. Rev.* **D94** (2016), no. 6 063505, [[arXiv:1605.08043](#)].
- [20] F. Bishara, J. Brod, B. Grinstein, and J. Zupan, *From quarks to nucleons in dark matter direct detection*, *JHEP* **11** (2017) 059, [[arXiv:1707.06998](#)].
- [21] S. Scopel and K. Yoon, *A systematic halo-independent analysis of direct detection data within the framework of Inelastic Dark Matter*, *JCAP* **1408** (2014) 060, [[arXiv:1405.0364](#)].
- [22] S. Scopel, K.-H. Yoon, and J.-H. Yoon, *Generalized spin-dependent WIMP-nucleus interactions and the DAMA modulation effect*, *JCAP* **1507** (2015), no. 07 041, [[arXiv:1505.01926](#)].
- [23] S. Kang, S. Scopel, G. Tomar, and J.-H. Yoon, *DAMA/LIBRA-phase2 in WIMP effective models*, *JCAP* **1807** (2018), no. 07 016, [[arXiv:1804.07528](#)].
- [24] S. Kang, S. Scopel, and G. Tomar, *Probing DAMA/LIBRA in the full parameter space of WIMP effective models of inelastic scattering*, *Phys. Rev.* **D99** (2019) 103019, [[arXiv:1902.09121](#)].
- [25] **COSINE-100** Collaboration, G. Adhikari et al., *Search for a Dark Matter-Induced Annual Modulation Signal in NaI(Tl) with the COSINE-100 Experiment*, *Phys. Rev. Lett.* **123** (2019), no. 3 031302, [[arXiv:1903.10098](#)].
- [26] **COSINE-100, The Sogang Phenomenology Group** Collaboration, G. Adhikari et al., *COSINE-100 and DAMA/LIBRA-phase2 in WIMP effective models*, *JCAP* **1906** (2019), no. 06 048, [[arXiv:1904.00128](#)].

- [27] J. Amaré et al., *First Results on Dark Matter Annual Modulation from the ANAIS-112 Experiment*, *Phys. Rev. Lett.* **123** (2019), no. 3 031301, [[arXiv:1903.03973](#)].
- [28] A. L. Fitzpatrick, W. Haxton, E. Katz, N. Lubbers, and Y. Xu, *The Effective Field Theory of Dark Matter Direct Detection*, *JCAP* **1302** (2013) 004, [[arXiv:1203.3542](#)].
- [29] N. Anand, A. L. Fitzpatrick, and W. C. Haxton, *Weakly interacting massive particle-nucleus elastic scattering response*, *Phys. Rev.* **C89** (2014), no. 6 065501, [[arXiv:1308.6288](#)].
- [30] R. Catena, A. Ibarra, and S. Wild, *DAMA confronts null searches in the effective theory of dark matter-nucleon interactions*, *JCAP* **1605** (2016), no. 05 039, [[arXiv:1602.04074](#)].
- [31] J. Goodman, M. Ibe, A. Rajaraman, W. Shepherd, T. M. P. Tait, and H.-B. Yu, *Constraints on Dark Matter from Colliders*, *Phys. Rev.* **D82** (2010) 116010, [[arXiv:1008.1783](#)].
- [32] M. R. Buckley, *Using Effective Operators to Understand CoGeNT and CDMS-Si Signals*, *Phys. Rev.* **D88** (2013), no. 5 055028, [[arXiv:1308.4146](#)].
- [33] A. De Simone and T. Jacques, *Simplified models vs. effective field theory approaches in dark matter searches*, *Eur. Phys. J.* **C76** (2016), no. 7 367, [[arXiv:1603.08002](#)].
- [34] A. Belyaev, E. Bertuzzo, C. Caniu Barros, O. Eboli, G. Grilli Di Cortona, F. Iocco, and A. Pukhov, *Interplay of the LHC and non-LHC Dark Matter searches in the Effective Field Theory approach*, *Phys. Rev.* **D99** (2019), no. 1 015006, [[arXiv:1807.03817](#)].
- [35] J. Brod, A. Gootjes-Dreesbach, M. Tamaro, and J. Zupan, *Effective Field Theory for Dark Matter Direct Detection up to Dimension Seven*, *JHEP* **10** (2018) 065, [[arXiv:1710.10218](#)].
- [36] S. Kang, S. Scopel, G. Tomar, and J.-H. Yoon, *On the sensitivity of present direct detection experiments to WIMP-quark and WIMP-gluon effective interactions: A systematic assessment and new model-independent approaches*, *Astropart. Phys.* **114** (2020) 80–91, [[arXiv:1810.00607](#)].
- [37] E. Del Nobile, *Complete Lorentz-to-Galileo dictionary for direct dark matter detection*, *Phys. Rev.* **D98** (2018), no. 12 123003, [[arXiv:1806.01291](#)].
- [38] E. Del Nobile, G. B. Gelmini, P. Gondolo, and J.-H. Huh, *Direct detection of Light Anapole and Magnetic Dipole DM*, *JCAP* **1406** (2014) 002, [[arXiv:1401.4508](#)].
- [39] S. Kang, S. Scopel, G. Tomar, J.-H. Yoon, and P. Gondolo, *Anapole Dark Matter after DAMA/LIBRA-phase2*, *JCAP* **1811** (2018), no. 11 040, [[arXiv:1808.04112](#)].
- [40] F. Bishara, J. Brod, B. Grinstein, and J. Zupan, *DirectDM: a tool for dark matter direct detection*, [[arXiv:1708.02678](#)].
- [41] S. Kang, S. Scopel, G. Tomar, and J.-H. Yoon, *Present and projected sensitivities of Dark Matter direct detection experiments to effective WIMP-nucleus couplings*, *Astropart. Phys.* **109** (2019) 50–68, [[arXiv:1805.06113](#)].
- [42] R. Catena and B. Schwabe, *Form factors for dark matter capture by the Sun in effective theories*, *JCAP* **1504** (2015), no. 04 042, [[arXiv:1501.03729](#)].
- [43] S. E. Koposov, H.-W. Rix, and D. W. Hogg, *Constraining the Milky Way potential with a 6-D phase-space map of the GD-1 stellar stream*, *Astrophys. J.* **712** (2010) 260–273, [[arXiv:0907.1085](#)].

- [44] T. Piffi et al., *The RAVE survey: the Galactic escape speed and the mass of the Milky Way*, *Astron. Astrophys.* **562** (2014) A91, [[arXiv:1309.4293](#)].
- [45] E. Del Nobile, G. Gelmini, P. Gondolo, and J.-H. Huh, *Generalized Halo Independent Comparison of Direct Dark Matter Detection Data*, *JCAP* **1310** (2013) 048, [[arXiv:1306.5273](#)].
- [46] R. Bernabei et al., *Searching for WIMPs by the annual modulation signature*, *Phys. Lett.* **B424** (1998) 195–201.
- [47] **DAMA** Collaboration, R. Bernabei et al., *First results from DAMA/LIBRA and the combined results with DAMA/NaI*, *Eur. Phys. J.* **C56** (2008) 333–355, [[arXiv:0804.2741](#)].
- [48] **DAMA, LIBRA** Collaboration, R. Bernabei et al., *New results from DAMA/LIBRA*, *Eur. Phys. J.* **C67** (2010) 39–49, [[arXiv:1002.1028](#)].
- [49] R. Bernabei et al., *First Model Independent Results from DAMA/LIBRA-Phase2*, *Universe* **4** (2018), no. 11 116, [[arXiv:1805.10486](#)]. [*At. Energ.*19,307(2018)].
- [50] S. Baum, K. Freese, and C. Kelso, *Dark Matter implications of DAMA/LIBRA-phase2 results*, *Phys. Lett.* **B789** (2019) 262–269, [[arXiv:1804.01231](#)].
- [51] G. Angloher et al., *The COSINUS project - perspectives of a NaI scintillating calorimeter for dark matter search*, *Eur. Phys. J.* **C76** (2016), no. 8 441, [[arXiv:1603.02214](#)].
- [52] F. Kahlhoefer, F. Reindl, K. Schöffner, K. Schmidt-Hoberg, and S. Wild, *Model-independent comparison of annual modulation and total rate with direct detection experiments*, *JCAP* **1805** (2018), no. 05 074, [[arXiv:1802.10175](#)].
- [53] **XENON** Collaboration, E. Aprile et al., *Dark Matter Search Results from a One Ton-Year Exposure of XENON1T*, *Phys. Rev. Lett.* **121** (2018), no. 11 111302, [[arXiv:1805.12562](#)].
- [54] **PICO** Collaboration, C. Amole et al., *Dark Matter Search Results from the Complete Exposure of the PICO-60 C₃F₈ Bubble Chamber*, *Phys. Rev.* **D100** (2019), no. 2 022001, [[arXiv:1902.04031](#)].
- [55] **XENON** Collaboration, E. Aprile et al., *Signal Yields of keV Electronic Recoils and Their Discrimination from Nuclear Recoils in Liquid Xenon*, *Phys. Rev.* **D97** (2018), no. 9 092007, [[arXiv:1709.10149](#)].
- [56] **XENON100** Collaboration, E. Aprile et al., *Likelihood Approach to the First Dark Matter Results from XENON100*, *Phys. Rev.* **D84** (2011) 052003, [[arXiv:1103.0303](#)].